Arab J. Nucl. Sci. Appl., Vol. 52, 2, 103-111 (2019)

Arab Journal of Nuclear Sciences and Applications

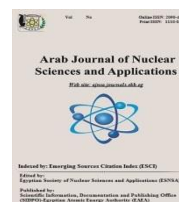

ISSN 1110-0451 ***Web site: ajnsa.journals.ekb.eg*** **(ESNSA)**

Microstructure, Creep Deformation Behavior and Reliability of Sn-6.5wt%Zn-0.3 wt% Cu Lead Free Solder after Bi Additions

E.H. El-Khawas, M.M. Fadel
Basic Science Department, Higher Technological Institute, Tenth of Ramadan City, Egypt

Received 7th Aug. 2018
Accepted 5th Mar. 2019

Creep characteristics of Sn-6.5 Zn-0.3 Cu plain solder was studied and compared with Sn-6.5 Zn-0.3 Cu-1 Bi and Sn-6.5 Zn-0.3 Cu-3 Bi solder alloys. The results show that 3Bi-containing alloy solder has the higher creep resistance (~80 times) than the other two solders at the same stress level and testing temperatures. The higher creep resistance was attributed to the solid solution and precipitations strengthening effects of Bi atoms. The precipitation of Bi atoms or particles can significantly refine the microstructure, blocks the movement of dislocations and increases the creep resistance of Bi-containing solders. Moreover, the creep life time of plain SZC plain solder alloy was extremely enlarged (~23.7 times) with the addition of 3 wt. % Bi, which could result in improving the reliability of Bi-containing solders. Additionally, the minimum creep strain rate in the steady state flow is developed during secondary creep and Garofalo model was created from the experimental data to predict the creep deformation mechanism. Based on the obtained stress exponents and activation energies, it is proposed that the dominant deformation mechanism is dislocation climb over the whole temperature range investigated.

Keywords; Sn-6.5Zn solder alloy, Microstructure, Tensile creep properties

Introduction

It is well known that soldering represents an imperative joining method in the electronics industry and has been widely used for the joining of the modules and printed circuit boards. Recently, Sn-Pb solder was widely used in these applications. The popularity of this alloy is due to its relatively low melting point, cantankerous bonding characteristics, good wicking tendencies, good electrical continuity and low cost [1]. However, medical studies have shown that lead is a heavy metal toxin that can damage the kidneys, liver, blood and the central nervous system. This has prompted the development of Pb-free solders and has enhanced the research activities in this field. Another reason for the lead-free solder development is that the traditional tin-lead solders would no longer satisfy the increased functionality and miniaturization of modern electronic and optoelectronic components at more stringent operational temperatures and stresses. For example, the homologue temperature of soldered interconnections in service conditions can be as high as $0.8T_m$, although the pitch and joint size of solder joints turn to be ever smaller. In these cases, there is an imperative requirement of high performance interconnection and packaging, such as excellent creep resistance and high size stability of packaged systems. In the recent decade, a great amount of effort has been devoted to the search for appropriate lead-free solders, which are expected to have satisfied processing performance, mechanical and physical properties comparable to traditional Sn–Pb solders [2–6]. For the lead free solders in electronic packaging applications, the melting temperature of solders and the

Corresponding author: enash12@hotmail.com , enash12@hti.edu
DOI: ***10.21608/ajnsa.2019.4731.1109***
© Scientific Information, Documentation and Publishing Office (SIDPO)-EAEA

fundamental performance characteristics of solder are a pronounced concern. For these applications, the melting temperature of solder determines the maximum allowable temperature that the devices and substrates can be exposed to in service. There is a commonly asked question, that is, which of these lead-free solders would be the most appropriate for the replacement of traditional tin-lead solders. But it is not easy to give simple answers since there is no absolute drop in replacement for Sn–Pb solders with identical melting-point, wetting performance, mechanical properties and cost [7].

Currently, there are several promising candidate lead-free solders for consideration in different applications. Among these lead-free candidate solders, the near ternary eutectic Sn–Zn–Cu system solders with melting temperature around 202 ^{o}C, are used for low temperature applications. However, the melting temperature of Sn–Zn–Cu system solder is over 19 ^{o}C higher than that of Sn–Pb eutectic and near-eutectic solders (~183°C). Thus, it is expected to improve the processing performance of Sn–Zn–Cu system solders by lowering its melting temperature and decreasing the surface tension of solder during melting. Some studies had shown that the addition of a small amount of Bi to Sn-based solders could reduce melting temperature [8], decrease surface tension and thus improve processing performance of the solder [9]. However, the addition of bismuth may also result in brittleness of the solder and deteriorate the mechanical property of soldered joint. Moreover, Sn-Zn-based solders were found to be useful in joining of copper [10]. The γ-Cu_5Zn_8 phase is the only one that was found at the eutectic Sn-Zn-Cu composition. Other studies [11-12] found up to three intermetallic (IMC) layers at the interface: ε-CuZn5, γ-Cu5Zn_8, and β-CuZn.

In this study, amounts of Bi element (1.0–3.0% wt %) were added to the lead-free Sn–6.5 wt% Zn–0.3 wr% Cu (SZC plain solder) to obtain Sn-6.5Zn-0.3Cu-1Bi and Sn-6.5 Zn-0.3 Cu-3 Bi solder alloys. Systematic investigations on the evolution of microstructure, distribution of the alloy phases, thermal, and creep properties have been carried out at different temperatures (25, 50, 75, 90 and 110°C) under the effect of different applied stresses to further understand the strengthen mechanism of new solders.

Experimental Work

Commercially pure Sn, Zn, Cu and Bi (99.98 wt.%) were used as raw materials to elaborate the proposed plain Sn-6.5 wt% Zn-0.3 wt% Cu solder and Bi-containing solders; Sn-6.5 wt% Zn-0.3 wt% Cu-1 wt% Bi and Sn-6.5 wt% Zn-0.3 wt% Cu-3 wt% Bi, hereafter is called SZC, SZC-1 Bi and SZC-3 Bi alloys, respectively. The process of melting of appropriate weights of Sn, Zn, Bi and Cu was carried out in a resistance type furnace at 700 ^{o}C for 70 min, and then poured in a steel mold to prepare a chill cast ingot. Chemical compositions of the three solders are shown in Table (1).

Characterization of microstructure evolution was carried out using scanning electron microscopy (SEM) Philips XL-30 microscope, which was coupled with an energy dispersive spectroscopy unit (EDS). A solution of 2% HCL, 3% HNO_3 and 95 % (vol %) Ethyl alcohol was prepared and used to each sample. Phase identification of the alloy samples was carried out using X ray diffractometer (XRD) at 40 kV and 20 mA using Cu Kα radiation with diffraction angle from 10° to 100° and a constant scanning speed of 10 min^{-1}. The homogenized cast ingots were then mechanically machined into wire samples with a gauge length marked 4 x 10^{-2} m for each samples and 1.2 x 10^{-3} m diameter. To obtain Samples containing the fully precipitated phases and free from plastic strain accumulation during machining, these samples were annealed at 120°C for 60 min, then left to cool slowly to room temperature. The environment chamber temperature could be monitored by temperature control using a thermocouple contacting with the tested sample. Then, the tensile tests results were obtained by averaging testing data. Tensile creep tests were conducted using a computerized tensile creep testing machine at a temperature range of 20-110°C, under different constant loads.

Results and Discussion

Microstructure analysis

XRD was conducted to identify the phase structures of SZC, SZC-1 Bi and SZC-3 Bi alloys solder and the corresponding patterns are presented in Fig. (1). As seen, three types of phases: β-Sn, Cu_6Sn_5 and CuZn were detected in the three alloys. Besides, the diffraction patterns of three solders are found to have nearly the same features. However, Fig. (1c) shows that new peaks are detected only with the addition of 3 wt.% Bi into

the SZC solder alloy. This implies that the 1 wt.% Bi content of the alloy predominantly dissolves in the β-Sn matrix to form a solid solution, whereas 3 wt.% Bi content could result in precipitated of Bi particles.

Table (1): Chemical composition of three solders studied (wt. %)

Alloy	Zn	Cu	Fe	As	Pb	Bi	In	Sn
Sn-6.5Zn-0.3Cu	6.507	0.301	0.003	0.002	0.002	0.00	0.002	Bal
Sn-6.5Zn-0.3Cu-1Bi	6.503	0.303	0.003	0.002	0.003	1.02	0.002	Bal
Sn-6.5Zn-0.3Cu-3Bi	6.505	0.302	0.003	0.002	0.003	3.04	0.002	Bal

SEM micrographs for the microstructure of plain solder and two Bi-containing solders are shown in Fig. (2). In Figure (2a), the structure of bulk SZC plain solder shows a primary β-Sn phase and coarse needle-like structure of αZn phase dispersed within the β-Sn matrix. Besides, Cu6Sn5 and Cu5Zn8 phases were also detected by XRD as shown in Fig. (1). The addition of Bi altered the microstructure of SZC plain solder. Figure (2b) illustrates that the coarse needle-like structure of αZn phase is refined after 1 wt% Bi addition. As seen, the light gray needle-like structure of Zn phase is finely dispersed in β-Sn matrix, while the dark gray area of plate-like structure is identified as Cu6Sn5 and Cu5Zn8 phases. The chemical compositions of the phases are confirmed by the EDS analysis shown in Figs. (2 d and e). Moreover, the addition of 3 wt% Bi could result in white cluster shaped Bi precipitates, since the solubility of Bi in Sn is about 1.0 at % at room temperature. These particle-dispersed regions are separated by regions of Sn, giving the microstructure a network-type appearance. There were no obvious microstructural differences among the solder alloys, except the refinement of Cu_5Zn_8 (Fig. 2c compared with that in Fig. 2b). The microstructure of Bi-containing alloys varies in terms of particles morphology, and is expected to overall impact on the mechanical properties as will be clarified in the following section.

Tensile creep response

It is well known that the microstructure characteristics of an alloy determine its mechanical response. To evaluate the tensile creep response of the plain SZC, SZC-1 wt% Bi and SZC-3 wt% Bi solders, tensile creep tests were carried out at the temperatures 20, 50, 70, 90 and 110°C under the effect of different applied stresses ranging from 15.59 to 27.28 MPa. Figure (3) shows the effect of Bi additions with different concentrations on the tensile creep of SZC plain solder as illustrated in the representative creep curves Fig. (3) for samples tested at 25oC under the effect of 15.59- 27.28 MPa.

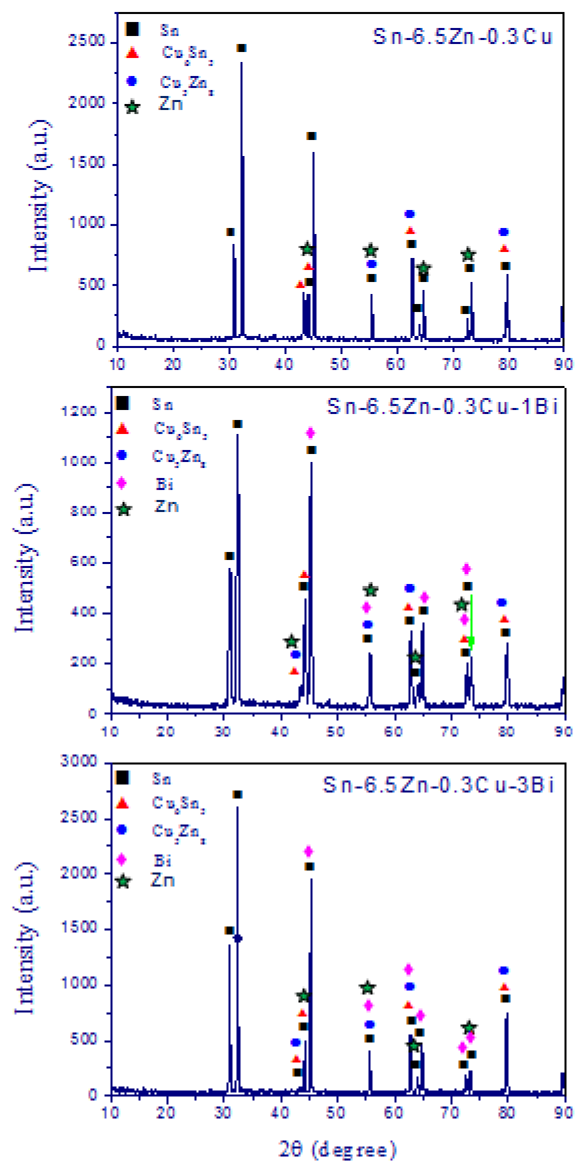

Fig. (1): XRD pattern for (a) the plain SZC, (b) SZC-1 Bi and (c) SZC-3Bi solder alloys

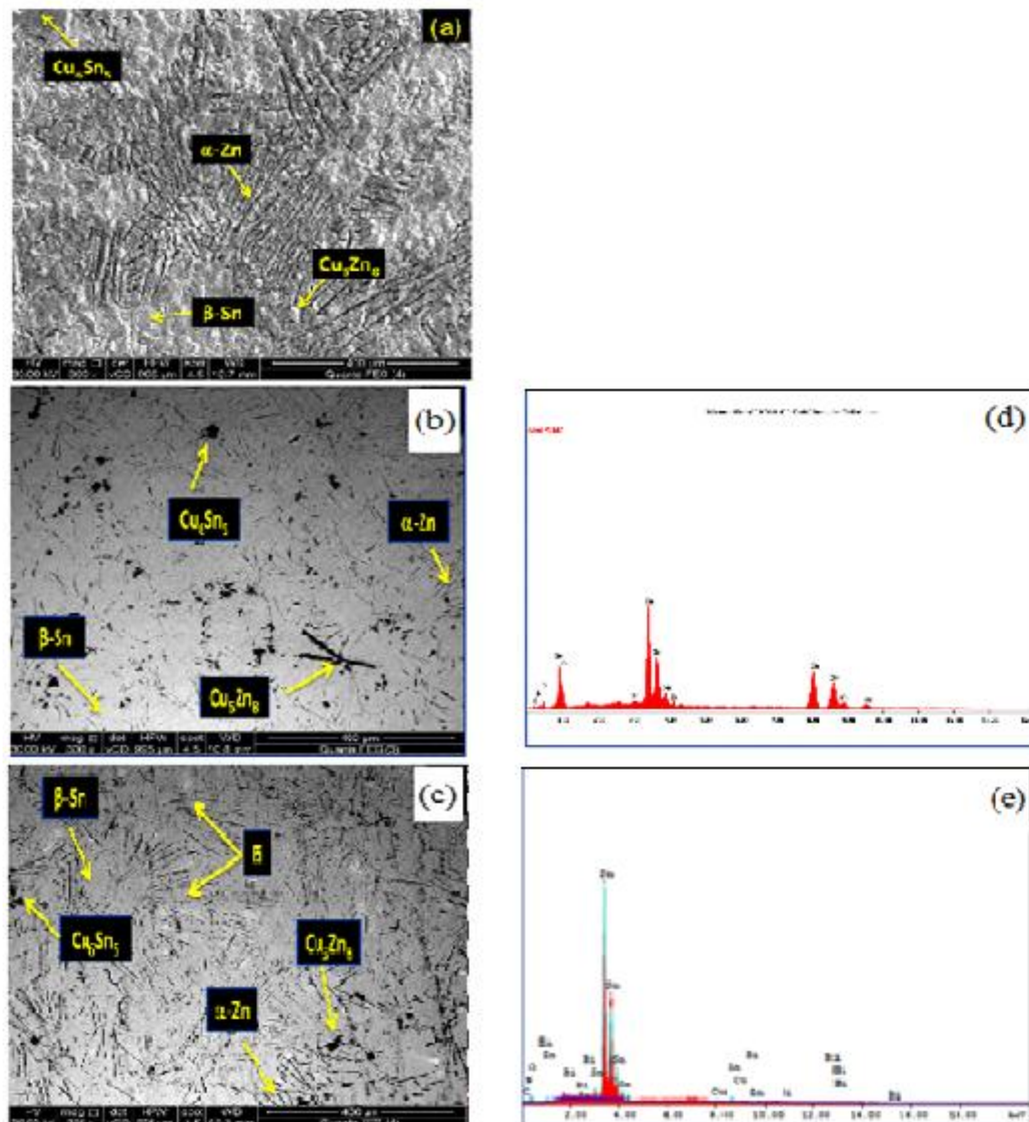

Fig. (2): SEM microstructures of (a) the plain SZC, (b) SZC-1 Bi and (c) SZC and SZC-3Bi solder alloys and corresponding EDS analysis (d) and (e)

It is clear that the Bi content greatly affects the creep rate of the tested samples. The creep resistance was drastically increased with increasing the Bi content. However, the creep rate was also found to be strongly affected by the test temperature and applied stress for the three solders. Figure (4) shows a set of representative creep curves for SZC-1wt%Bi stretched at 15.19 MPa and temperatures 20, 50, 70, 90 and 110oC, while Fig. (5) compares another set of representative creep curves for SZC plain solder tested at different temperatures under the effect of stresses ranging from 15.59 to 31.18 MPa.

From these Figures, it is clear that the creep curves are monotonic shifted towards higher strain rates and lower fracture times with increasing the deformation temperature Fig. (4) and/or applied stress Fig. (5) for the three solder alloys. To compare the creep resistance of the entire alloy samples, the strain rates are calculated. The average minimum creep rates ε. were 3.0 x 10-4 s-1 and 1.0 x 10-5 s-1 and 3.0 x 10-6 s-1 for the SZC-3 wt% Bi, SZC-1wt% Bi and plain solder, respectively. It indicated that the 3 wt% Bi-containing SZC solder has more creep resistant and more expected fracture time than that of 1 wt% Bi-containing SZC and plain solder at the same stress level and testing temperature. Since the stress and temperature are constants, the variations in the creep rate έ suggest a basic change in the

internal stress of the solder sample during creep test. As indicated in Fig. (3a), it could be noticed that the addition of 3 wt% Bi resulted in increasing creep resistance depending on the applied stress and testing temperature.

The minimum creep rate (ε.) is one of the most important parameters of creep resistance in engineering assessments. Comparing the three solder alloys, the creep rate ε. decreases and the creep rupture time tf is expected to increase significantly with increasing the Bi content at the same stress levels.

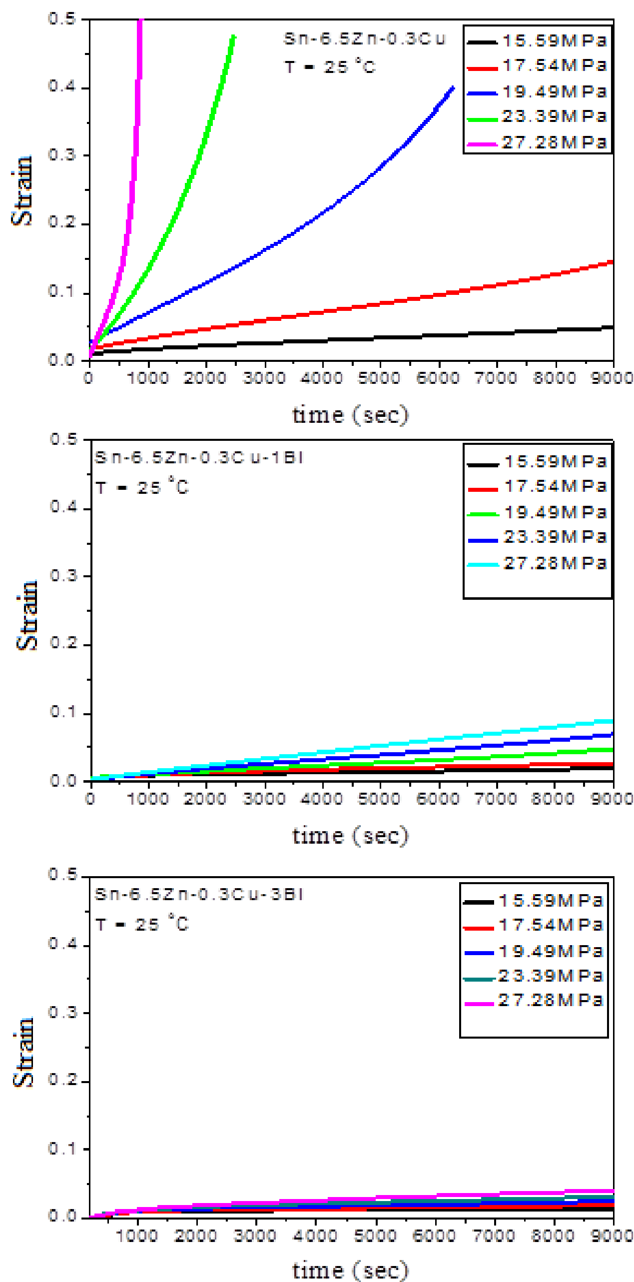

Fig. (3): Representative creep curves for the plain (SZC), (SZC1wt. % Bi) and (SZC 3 wt. % Bi) alloys test T=25 °C under different stresses

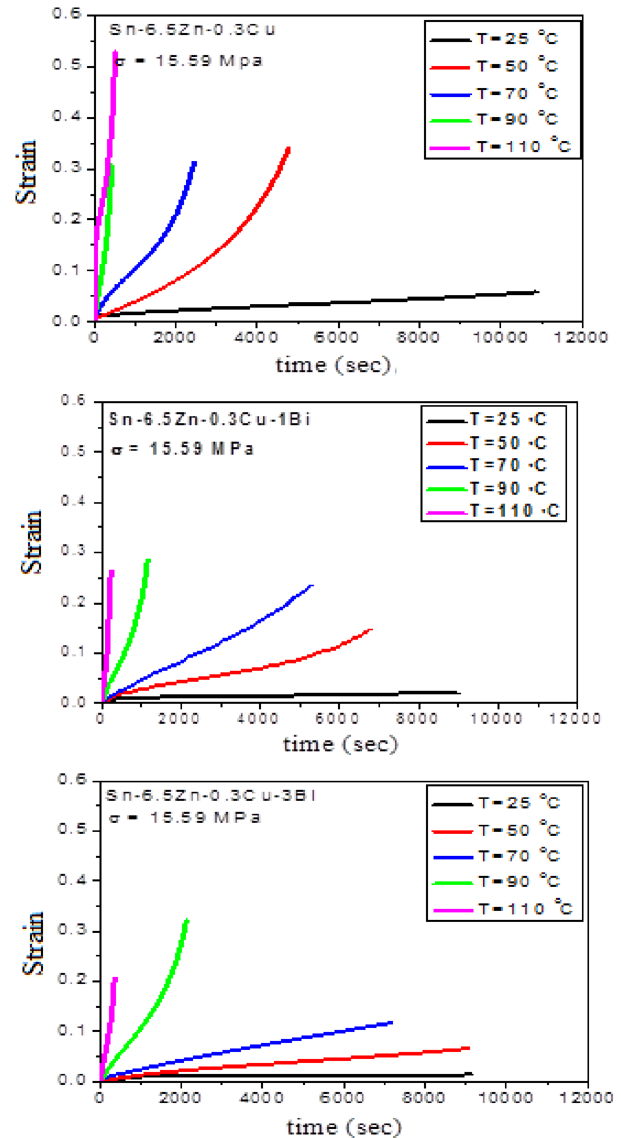

Fig. (4): Representative creep curves for the plain SZC, SZC-1wt. % Bi and SZC-3wt. % Bi alloys tested at σ =15.59 MPa under different temperatures

The high creep resistance of Bi-containing SZC solder is mainly attributed to the solid solution effect of the Bi atoms as well as the precipitated Bi particles Fig. (3c), since the strengthening effects of the Bi particles increased the creep resistance of SZC-1wt% Bi and SZC-3 wt% Bi solder alloys. With the precipitation of fine Bi particles, not only the dislocation gliding the distance between these particles, but also the climbing and by-passing forces of dislocation, have been changed. The Orowan bowing stress, which is related to the dislocation climb and by-passing particles, increases with the decrease of particle size and

inter-particle distance. It is indicated that the SZC-3 wt% Bi alloy has about 80 times creep resistance higher than SZC plain solder at the same stress level and testing temperature. Moreover, the creep life time of the plain SZC alloy is expected to be extremely enlarged (about 23.7 times).

Constitutive creep equation and parameters of lead-free solder alloys

For the vast majority of applications in metals and alloys, the steady-state creep stage arrests the most of creep time to final failure at homologous temperatures greater than half the absolute melting temperature (TH > 0.5Tm). In the steady-state stage, the minimum creep rate ε.m as a function of temperature T, activation energy Q and stress σ can be expressed by Dorn Power Law [13-14]:

$$\dot{\varepsilon} = A\, \sigma^{n1} \exp(-Q/RT) \quad (1)$$

Where R is the universal gas constant, A is a material constant. The creep stress exponent, n1, and activation energy of diffusion, Q, are the two essential mechanical and thermodynamic parameters for describing creep behavior. The n1 value in creep models denotes the contribution of applied stress effects on creep deformation. The activation energy represents the height of energy barrier, which the atoms have to overcome to diffuse and disperse to lower energy levels. Eq. (1) cannot span both the power law equation and exponential equation, respectively. Since the power, law equation breaks down at high stress values, while the exponential equation breaks down at low stress values. The following Garofalo hyperbolic-sine law is accepted to be the most appropriate form for explaining the creep deformation behavior over a wide range of stresses:

$$\dot{\varepsilon} = A\, [\sinh(\alpha\sigma)]^{n} \exp(-Q/RT) \quad (2)$$

Equation (2) does not obviously partition the low- and high-stress creep mechanisms, but fairly treats steady state creep with an effective or apparent activation energy that may represent multiple creep mechanisms. The creep rate is determined by taking the natural logarithmic transformation on both sides of Eq. (2), and then we have,

$$\ln\dot{\varepsilon} = \ln A + n \ln[\sinh(\alpha\sigma)] - (Q/RT) \quad (3)$$

Where α is the stress reciprocal at which the material deformation changes from power to exponential stress dependence. The n value denotes the sensitivity of the steady state creep to applied stress. The value of α was calculated by the equation: α = β/n1, where β and n1 are the average slopes of lnε.- σ lines Fig. (6) and lnε.- lnσ lines Fig. (7). Slopes of the lnε.- against ln [sinh (ασ)] plot Fig. (9) gave values of n Table (2). The value of lnA could then be obtained from the intercept of the lnε.- against ln [sinh (ασ)] Fig. (8). The creep-activation energy Q of the entire solders can be approximately calculated in the temperature range 25–110 oC, by linear regression of the experimental data relating lnε. and 1/T Fig. (9). The parameters are summarized in Table (2). These summaries reveal a range of n and Q values due to the differences in microstructural features shown in Fig. (3). It is well known that the n value increases progressively with increasing creep resistance and decreases at higher deformation temperatures [15, 16].

Notably, the measured values of n shown in Table (2) and Fig. (8) illustrate the same tendency. As expected, the creep resistance of the three alloys was highest at 25 oC, while it decreased with increasing deformation temperature. For SZC, SZC-1Bi and SZC-3 Bi solders, the n value decreased from 4.5 to 4.1, from 5.0 to 4.3, and from 5.4 to 4.6, respectively, as the temperature increases from 25 to 110 oC as illustrated in Table (2). However, the slight decrease in n values with increasing temperature confirms the comparatively higher stability of these solders at high temperatures than the other lead-free solder alloys [12, 16-18]. Moreover, the present study illustrates the increase of n value with increasing Bi content in SZC based-solders. The higher the stress exponent, the better the strengthening effect of the second phases in alloy matrix, and the greater the creep resistance is. For the present lead-free Sn–Ag–Cu–Bi solder, the calculated creep-activation energy is 77.8 kJ/mol for SZC-3wr%Bi, 72kJ/mol for SZC-1 wt%% Bi and 61.5 kJ/mol for the SZC plain solder which is somewhat larger than those obtained for the Sn60Pn40 solder [19]. Finally, the creep stress exponent and activation energy values calculated for SZC plain, SZC-1Bi and SZC-3Bi solder alloys are reasonably close to other published data for Sn-based solder alloys

The creep mechanism in case of particle-strengthened or multiphase eutectic structures of Pb-free alloys seems to be similar to those observed in pure tin, but can operate at higher stress than in pure Sn. This corresponds to a mechanism of dislocation climb over the precipitate Bi particles as well as Ag3Sn and Cu6Sn5 IMCs in SAC led free solder alloys [13].

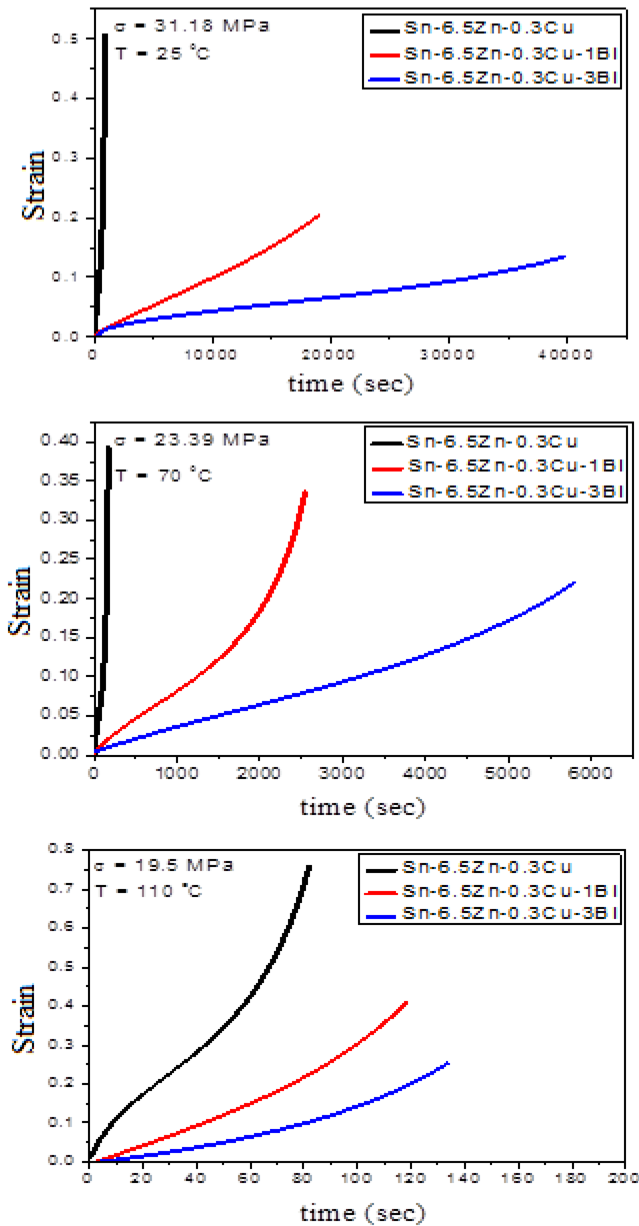

Fig. (5): Comparison of creep curves at (a) T=25ºC, σ=31.18 MPa, (b) T=70ºC, σ=23.39 MPa and (c) T=110ºC, σ=19.5 MPa for the plain SZC, SZC-1 wt.% Bi and SZC-3 wt.% Bi solder alloys

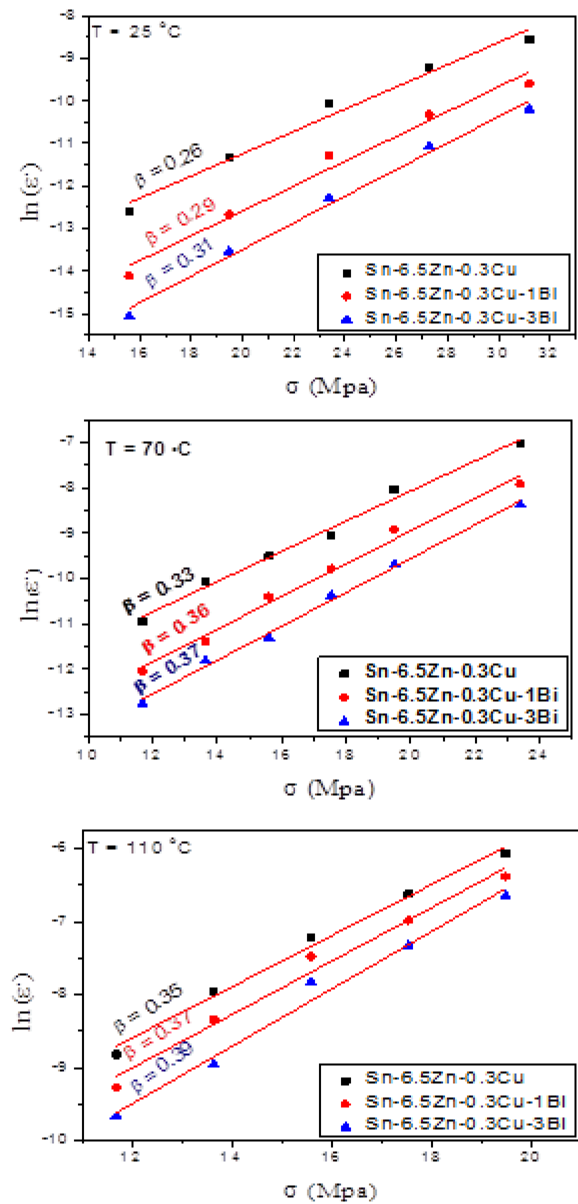

Fig. (6): Relationship between and ln(ε̇) and relationship between (α) and ln(ε̇) at T=25, T=70 and T=110°C for the plain SZC, SZC-1 Bi and SZC-3 Bi solder alloys

Table (2): Activation energy (Q), stress exponent (n) and (α) values for Sn–6.5Zn–0.3Cu, Sn–6.5Zn–0.3Cu–1Bi and Sn–6.5Zn–0.3Cu–3Bi solder alloys

Alloy	Q (kJ/mol)	Temperature (°C)	α	n
Sn-6.5Zn-0.3Cu	61.5	25	0.04333	4.5
		70	0.05893	4.3
		110	0.06481	4.1
Sn-6.5Zn-0.3Cu-1Bi	72	25	0.04394	5
		70	0.06023	4.7
		110	0.06607	4.3
Sn-6.5Zn-0.3Cu-3Bi	78.7	25	0.04429	5.4
		70	0.05873	4.8
		110	0.06503	4.6

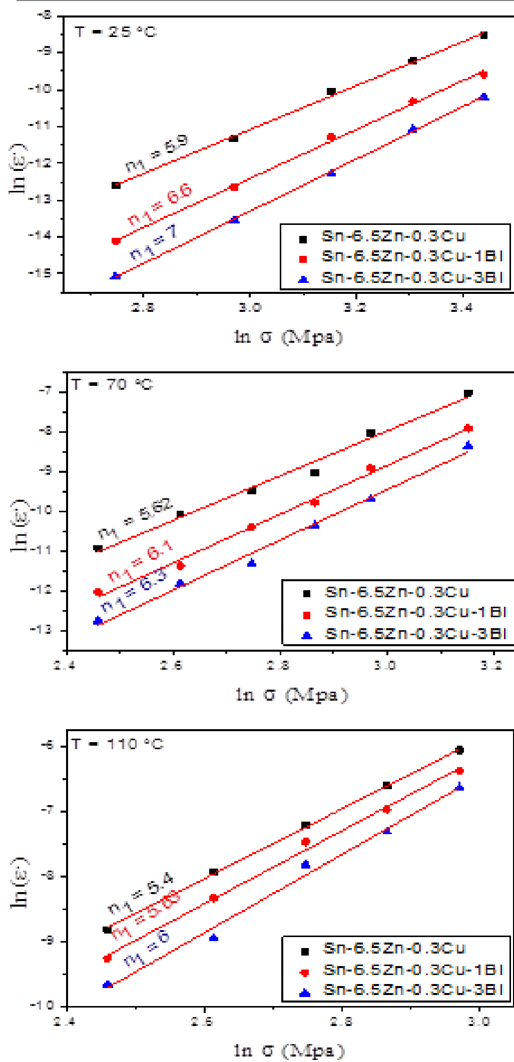

Fig. (7): Relationship between ln(α) and ln(ε˙) at T=25 , T=70 and T=110 °C for the plain SZC, SZC-1 wt.% Bi and SZC-3 wt.% Bi solder alloys

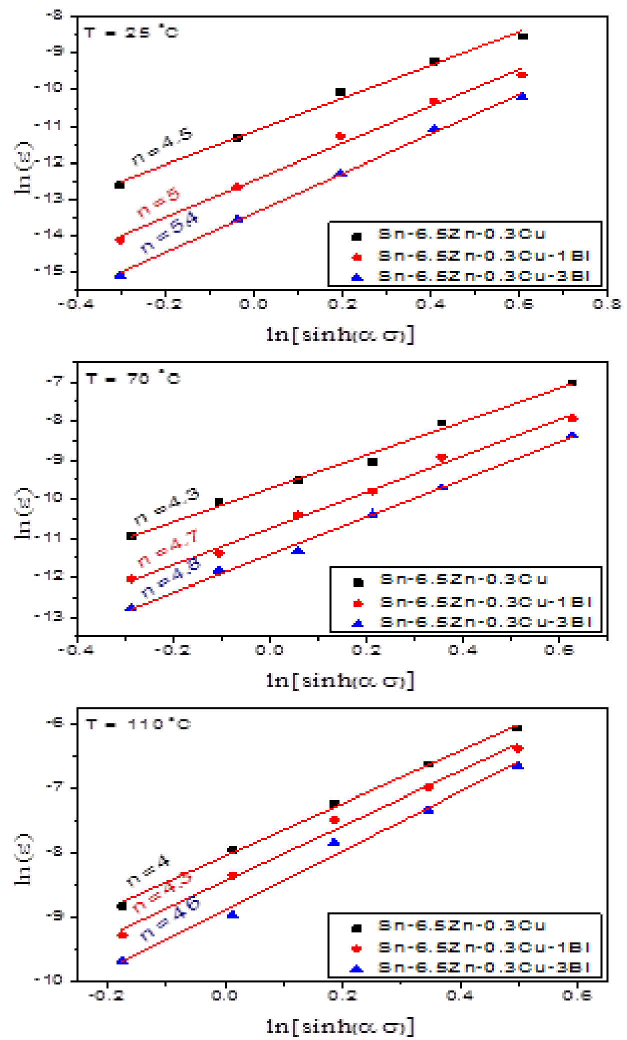

Fig. (8): Relationship between ln[sinh (ασ)] and ln) for determination the stress exponent values at T=25 , T=70 and T=110°C the plain SZC, SZC-1Bi and SZC-3 Bi solder alloys

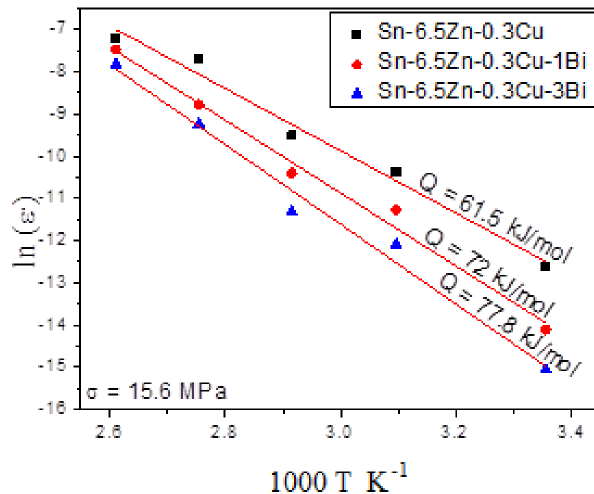

Fig. (9): The activation energy (Q) values of the plain SZC, SZC-1 Bi and SZC-3wt. Bi solder alloys

Conclusions

The microstructure, thermal and creep characteristics of different SZC plain, SZC-1wt% Bi and SZC-3 wt% Bi solder alloys were investigated.

The main conclusions are:

(1) With the addition of Bi, the microstructure of SZC plain solder is changed into fine needle-like Zn, dark Cu_6Sn_5 and Cu_5Zn_8 particles, which are uniformly distributed within the alloy matrix. Clusters of Bi particles were could be observed when Bi content is 3 wt.%.

(2) SZC-3 wt% Bi solder was found to have a higher creep resistance about 80 times greater than the SZC plain solder at the same stress level and testing temperature. The higher creep resistance was contributed by the solid solution and/or precipitations strengthening effects of Bi.

(3) The creep life time of SAC105 alloys was remarkably enhanced ~23.7 times with 3 wt.% Bi additions.

(4) The creep stress exponent and activation energy values calculated for SZC plain, SZC-1 Bi and SZC-3 Bi solder alloys in the steady-state creep regime fall well within the scope of other published data, where the proposed deformation mechanism is dislocation-pipe diffusion controlled climb over the whole temperature range investigated.

REFERENCES

1. M. Kamal, M.S. Mikhall, A.B. Bediwi and EL Said Gouda: Radiation Effects & Defects in Solids, 161(2006) 715–721.
2. U.R. Kattner, W.J. Boettinger, J. Electron. Mater. 23 (1994) 603.
3. X.P. Zhang, C. B. Yu, S. Shrestha, L. Dorn: J Mater Sci: Mater Electron 18 (2007) 665–670.
4. Ali Roshanghias, Johannes Bernardi, HerbertIpser; Materials Letters178 (2016)10–14.
5. S. Chou, S. Chen, and Y. Chang, J. Mater. Res., 21 (2006)1849–1856.
6. A. Hirose, H. Yanagawa, E. Ide, K.F. Kobayashi, Sci.Technol. Adv. Mater. 5 (2004) 267.
7. Przemysław Fima, Janusz Pstrus and Tomasz Gancarz; JMEPEG23 (2014) 1530–1535.
8. A. Hirose, H. Yanagawa, E. Ide, K.F. Kobayashi, Sci.Technol. Adv. Mater. 5 (2004) 267.
9. A.A. El-Daly, H.A. Hashem, N. Radwan, F. El-Tantawy, T.R. Dallou, N.A. Mansour. H.M. Abd-Elmoniem, E. H. Lotfy; J Mater Sci: Mater Electron 27(2016) 2950–2962.
10. X.P. Zhang, H.W. Wang, Y.W. Shi, J. Mater. Sci. - Mater. Electron. 15, (2004) 511.
11. A.A. El-Daly, A.M. El-Taher, S. Gouda; J. Alloys Compds; 627 (2015) 268–275.
12. A.A. El-Daly, A.M. El-Taher, T.R. Dalloul,; Mater. Des. 55 (2014) 309–318.
13. A.A. El-Daly, A.M. El-Taher, S. Gouda; Materials and Design 65 (2015) 796–805.
14. A.A El-Daly, A Fawzy, S. F Mansour, MJ Younis. J Mater Sci: Mater Electron 24 (2013) 2976–88.
15. E.S. Freitas, W.R. Osório, J.E. Spinelli, A. Garcia, Microelectron. Reliab. 54 (2014) 1392–1400.
16. A.A. El-Daly, A. E. Hammad, G. S. Al-Ganainy, M. Ragab, Mater. Sci. Eng. A 608 (2014) 130–138.
17. A.A. El-Dal y, A.M. El-Taher, T.R. Dalloul, J. Alloys Compds. 587 (2014) 32–39.
18. M.H. Braga, J. Vizdal, A. Kroupa, J. Ferreira, D. Soares, L. F. Malheiros, Calphad 31 (2007) 468–478.
19. X.P. Zhang, C.B. Yu و S. Shrestha, L. Dorn; J Mater Sci: Mater Electron 18 (2007)665–670.